Supporting Information

Microscopic *in-situ* Observation of Electromechanical Instability in Dielectric Elastomer Actuator Utilizing Transparent Carbon Nanotube Electrodes

Zhen-Qiang Song[a,d*], Li-Min Wang[a], Yongri Liang[a], Xiao-Dong Wang[b], Shijie Zhu[c*]

a. *Center for Advanced Structural Materials, State Key Laboratory of Metastable Materials Science and Technology, Yanshan University, China*

b. *School of Civil Engineering and Mechanics, Yanshan University, China*

c. *Department of Intelligent Mechanical Engineering, Fukuoka Institute of Technology, Japan*

d. *Hebei Key Lab for Optimizing Metal Product Technology and Performance, Yanshan University, China*

[*]Corresponding authors:

Zhen-Qiang Song, Email: zqsong@ysu.edu.cn

Shijie Zhu, Email: zhu@fit.ac.jp

The detailed EMI observation process is schematically shown in Fig. S1. The circular VHB 4905 elastomer with an initial thickness of 0.5 mm was equi-biaxially pre-stretched by a ratio of 1.5, and then fixed to a rigid annular frame cut from an acrylic plate. Two pieces of release paper (thickness of 0.02 mm) were arranged with a gap of 1 mm on the surface of the elastomer. Then, the filter membrane deposited with carbon nanotube (CNT) was stamped on the surface of the release paper, and carefully press the filter membrane to transfer the CNT to the gap region with a few drops of ethanol. The electrodes on opposite side were fabricated perpendicular to each other, forming a square area (1×1 mm^2) at the intersection. The elastomer membrane was fully relaxed for 0.5 hour before being positioned on the stage of Keyence VHX-600E microscope. The copper foil was utilized to connect the CNT electrodes to the power supply. The microscopic morphology of the active region was monitored and recorded as the voltage ramps up at a constant rate of 20 V/s.

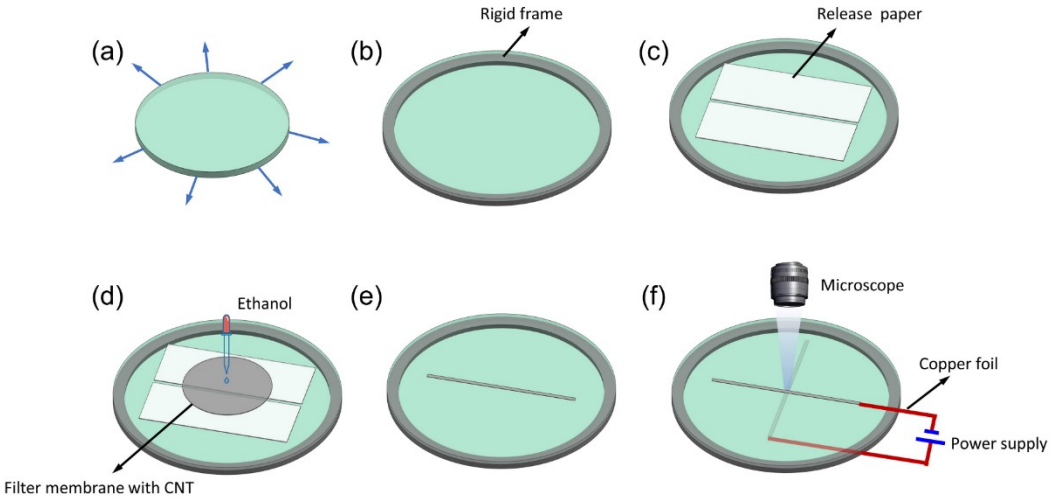

Fig. S1. The details for the EMI observation. (a) The VHB 4905 elastomer film was equi-biaxially pre-stretched. (b) The pre-stretched film was fixed on an annular rigid

frame. (c) Release paper was arranged with a gap of 1 mm. (d)-(e) The filter membrane deposited with carbon nanotube was stamped on the release paper, and ethanol was employed to transfer the CNT to the adhesive VHB 4905 surface at the gap. (f) The other CNT electrode on the opposite side of elastomer was prepared using a similar approach, and soft copper foil was utilized the connect the CNT electrodes to the power supply. The intersection region was *in-situ* monitored via Keynce VHX-600E microscope.

The equi-biaxial tension measurement was implemented on a customized test bench, as schematically shown in Fig. S2(a). The radial force was applied to the circumference of the DE membrane through 18 uniformly-distributed clips that was connected to the load cell and linear servo motor via stainless steel wires and pulleys (Fig. S2(b)). The membrane was stretched using a linear servomotor (GLM20AP, THK Co., Ltd), and the stretching force was measured with a load cell (U3B1-20K-B, Minebea Co., Ltd). The force data from load cell (F) and the displacement of the linear motor (s) were recorded by the LabVIEW software. The effective force (f) that is applied on the DE membrane was calculated as $F/\cos\varphi$, where φ is the half-angle between two opposite wires, given as $\varphi = arctan\frac{a}{b+s}$, with a and b were measured before stretching, as illustrated in Fig. S2 (c)-(d). The stretch ratio (λ) of the membrane was monitored by a high-resolution camera mounted over the elastomer during stretching process. Considering the viscoelasticity of VHB 4905 acrylic elastomer, the membrane was pre-stretched to a ratio of λ_{pre}=3 and fully-relaxed for 0.5 h, in

accordance with the testing conditions of DEAs in Fig. 5 of the main text.

The carbon nanotube electrode was fabricated following the procedures outlined in the Experimental Methods section, and the whole surfaces of the membrane were coated with SWCNT electrodes deposited with 1700 μL solution. Fig S3(a) shows the measured nominal stress plotted against stretch ratio of the elastomer coated with SWCNT, as well as carbon grease electrode as a reference. Fig S3(b) presents the voltage-stretch relationship calculated with the Eq. (S1), given as:

$$\sigma_{pre} + \varepsilon_0 \varepsilon_r \left(\frac{\Phi}{H}\right)^2 \lambda^3 = \sigma(\lambda) \tag{S1}$$

where the left two terms denote the pre-stretch stress at λ=3 and the Maxwell stress, respectively, and the right term is the measured elastic recovery stress of DE membrane in Fig. S3(a).

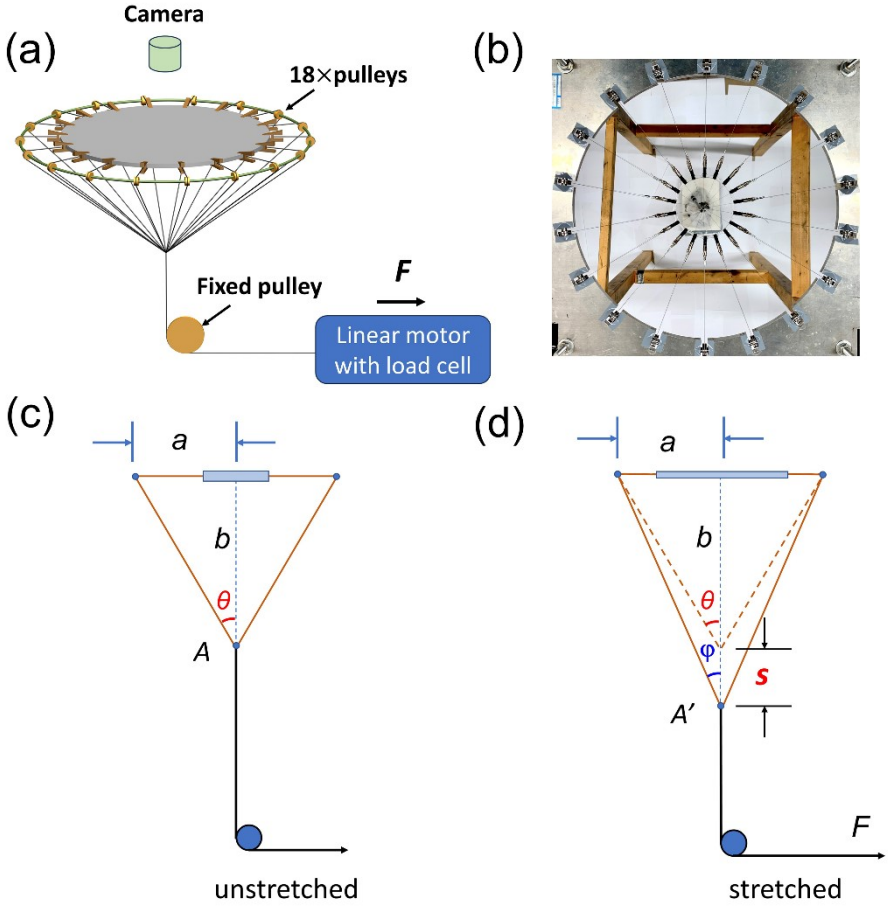

Fig. S2. (a) Schematics of equi-biaxial tension test for the dielectric elastomer membrane. (b) The photograph of the customized test bench employed in this study. (c) The membrane under unstretched state, with a is half distance between two pulleys diametrically opposite on the circle, b is initial distance between the wires knot and the elastomer membrane, and θ denotes the initial half-angle between two opposite wires. (d) The membrane under stretching state, with φ indicates the real-time half-angle between two opposite wires, and s is the stretching distance of the linear motor.

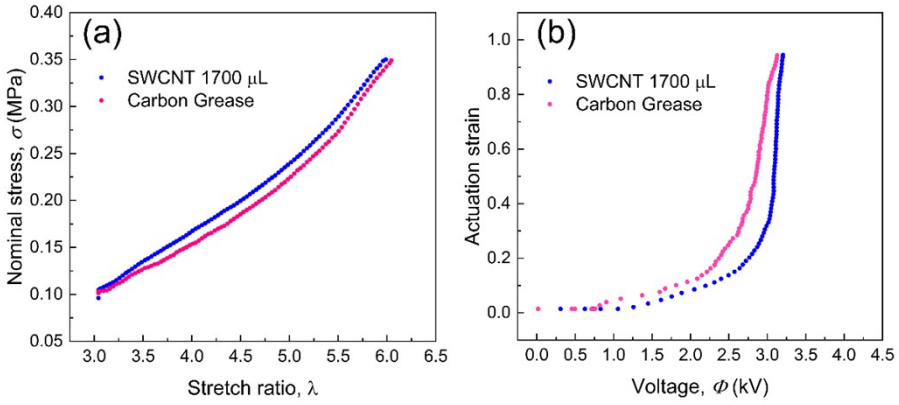

Fig. S3 (a) The measured nominal stress as a function of stretch ratio for the VHB 4905 elastomer coated with carbon grease and SWCNT electrodes. (b) The calculated actuation strain as a function of applied voltage utilizing the mechanical property data in image (a). This clearly demonstrates the stiffening effect of over thick SWCNT electrode, with the actuation plot shifting to a higher voltage level in image (b).

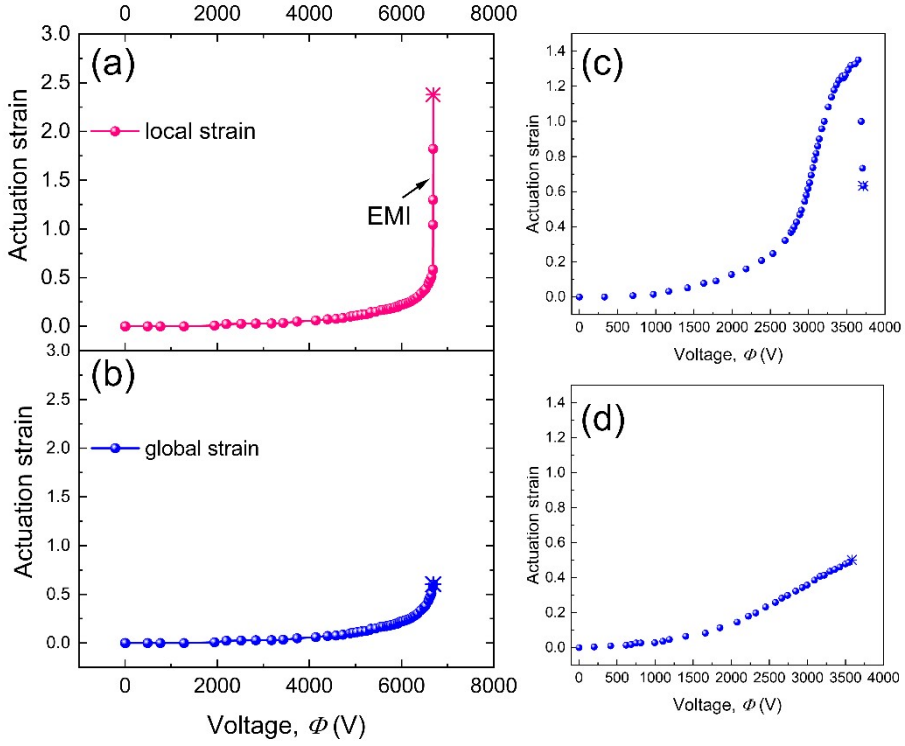

Fig. S4 The actuation strain, as measured from *in-situ* observations, is plotted against the driving voltage under the pre-stretch ratios of (a)-(b) λ_{pre}=1.5, (c) λ_{pre}=3 and (d)

λ_{pre}=5, respectively. For the case of λ_{pre}=1.5, a distinct strain bifurcation is discerned between (a) the localized instability domain and (b) the entire active region under high driving voltages. The asterisk symbols annotate the points of electrical breakdown.

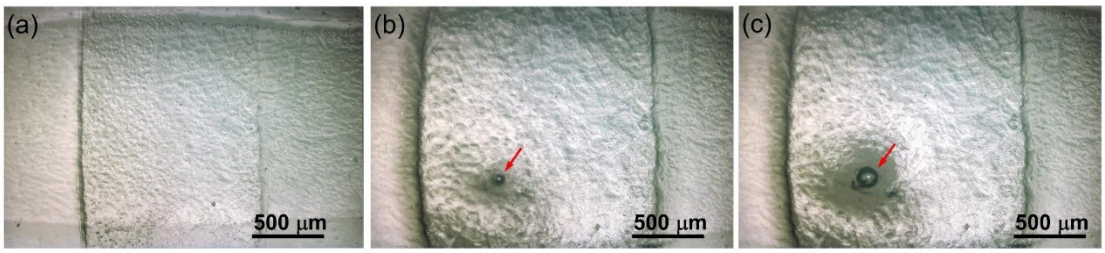

Fig. S5. The microscopic images of the active region under the pre-stretch of λ_{pre}=1.5 with the applied voltage of (a) 5938 V, (b) 6728 V and (c) 6730 V. The local EMI region away from the corner was denoted by the arrow.

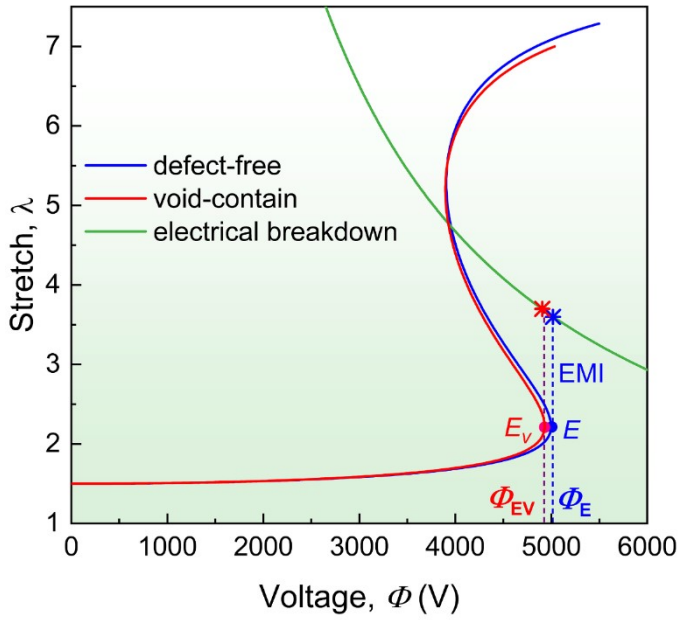

Fig. S6. The actuation plot of the defective region with the value of μ and J_m decreased by 3% due to the air void. The plot of defect-free elastomer was also presented for comparison.

The MSC Marc software was employed for the simulation. One spherical void or conductive particle (radius of 10 μm) was embedded in a circular dielectric elastomer with a diameter of 5 mm and a thickness of 0.5 mm, as shown in Fig. S7. Due to the axisymmetric nature of the DEA, only the cross section was modeled, and axisymmetric elements were adopted to ensure simulation accuracy. The dielectric elastomer material was characterized by the Gent model, with the small-strain shear modulus of 40 kPa and the first strain invariant of 125, and the relative permittivity is selected as 3.9. To exclude the stiffening effect of the electrode, it was modeled as a very soft material with the Young's modulus of 1 Pa. The air void was modeled as a fluid with the relative permittivity of 1, i.e. 8.85×10^{-12} F/m, while the conductive particle was modeled as a rigid material with Young's modulus of 200 GPa. The dielectric permittivity of the conductive material was set as 0.001 F/m. The relevant mechanical and dielectric parameters are listed in Table 1. The elastomer was pre-stretched by a ratio of 1.5, after which a voltage bias was applied on the electrodes.

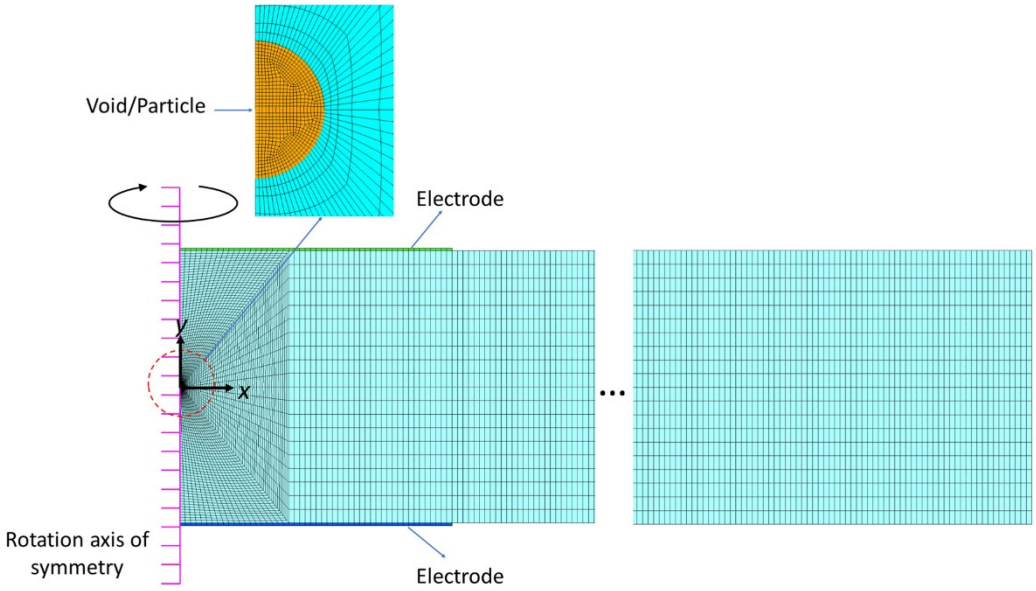

Fig. S7. Meshing of the model for the DEA embedded with an air void or conductive particle.

Table 1. The relevant mechanical and dielectric parameters for the FEA.

Materials	Mechanical parameter	Dielectric parameter (F/m)
Elastomer	Gent hyperelastic model (μ=40 kPa, J_m=125)	3.45×10^{-11}
Electrode	Young's modulus E=1 Pa	0.001
Air void	Fluid	8.85×10^{-12}
Conductive particle	Young's modulus E=200 GPa	0.001

For the air void inclusion, Fig. S8(a) presents the stress distribution after being stretched by a ratio of 1.5. It can be seen that the spherical void elongates in the *x*-

direction and contracts in the *y*-direction. The inset denotes the stress component in *x*-direction through the thickness, indicating that the stress concentration factor reaches approximately 1.87 at the top and bottom of boundary. Fig. S8(b) displays the electric field at the voltage of 3.6 kV. High electric intensity exists in the void due to its lower permittivity, whereas in the elastomer, the electric intensity around the void is generally lower than that in the matrix, except for a notable enhancement at the rightmost boundary location, where it measures approximately 2.4 times the nominal value in matrix. Additionally, the vector distribution map of electrical field exhibits a deviation from the vertical direction at the rightmost location, as illustrated by the inset.

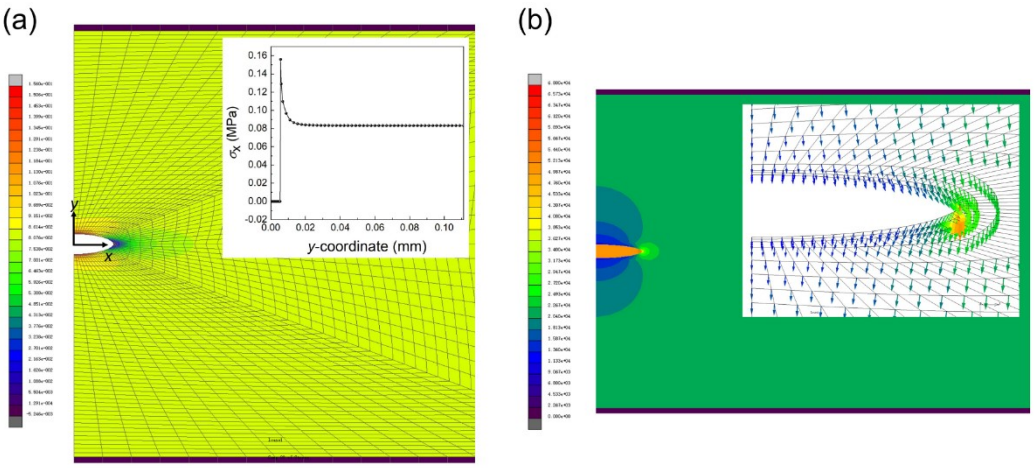

Fig. S8. The stress-electric field for DEA with air void inclusion. (a) The *x*-stress component distribution after being pre-stretched by a ratio of 1.5, and the inset shows the variation of σ_x as a function of *y*-coordinate. (b) The electric field distribution at the voltage of 3.6 kV, and the vector map around the void is shown by the inset. Please note that the mesh of the air-void is not shown in the data presentation of image (a) and inset of (b) for clarity.

Fig. S9(a) exhibits the *x*-stress component distribution for the particle inclusion after being stretched by a ratio of 1.5. The maximum stress located at about $\pm 54^\circ$ to the stretching direction. The electric field under the voltage of 3.6 kV is shown in Fig. S9(b). The electric field within the conductive particle is zero, while in the elastomer, remarkable electric field enhancement is observed around the particle, with the maximum value about 3.18 times the value in the matrix. However, the electric field nearly disappears at the rightmost boundary location, as indicated by the vector map in the inset.

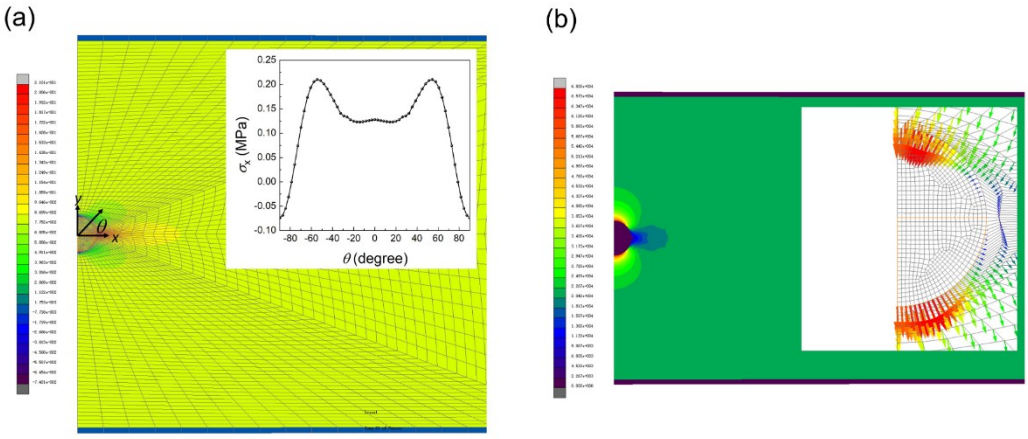

Fig. S9. The stress-electric field for the DEA with conductive particle inclusion. (a) The *x*-stress component distribution after being stretched by a ratio of 1.5. The inset indicates the value of σ_x along the boundary between the particle and matrix. (b) The electric field distribution at the voltage of 3.6 kV, and the vector map is shown by the inset.

Fig. S10 schematically shows the polymer networks under the (a) voltage-off, (b) voltage-on and (c) snap-through instability conditions of DEA, respectively. Initially, the polar groups are randomly oriented within the dielectric elastomer, as indicates in Fig. S10(a). As external voltage was applied, the orientation polarization takes place in the electric field, characterized by the dipole moments rotating towards to the same direction. During this process, opposite charges accumulate on the electrodes, and the electrostatic attractive force causes the membrane thinning in thickness and expansion in area, with the polymer chains shorten length in thickness and extend length in plane, as shown in Fig. S10(b). When the voltage is up to the critical value for electromechanical phase transition, local snap-through instability occurs with sudden thinning in thickness, which leads to the remarkable elongation of the polymer chains along the stretching direction. The ensuing electric field surge results in a more uniform orientation of the polar groups within the EMI region ("thin-phase") compared to the surrounding matrix ("thick-phase"), as shown in Fig. S10(c).

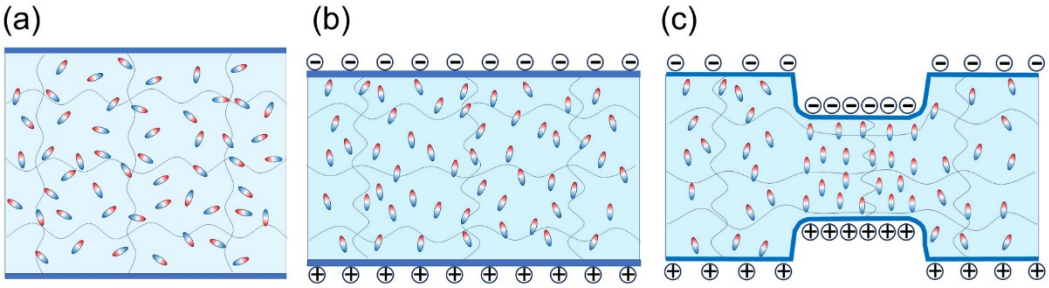

Fig. S10. (a) The elastomer under voltage-off condition, with the polar groups randomly oriented. (b) Orientation polarization occurs due to the applied electric field, and charges accumulate on the electrode. (c) Abrupt local thinning of the elastomer occurs due to the EMI, and a more uniform orientation of the polar groups forms within the

EMI region.

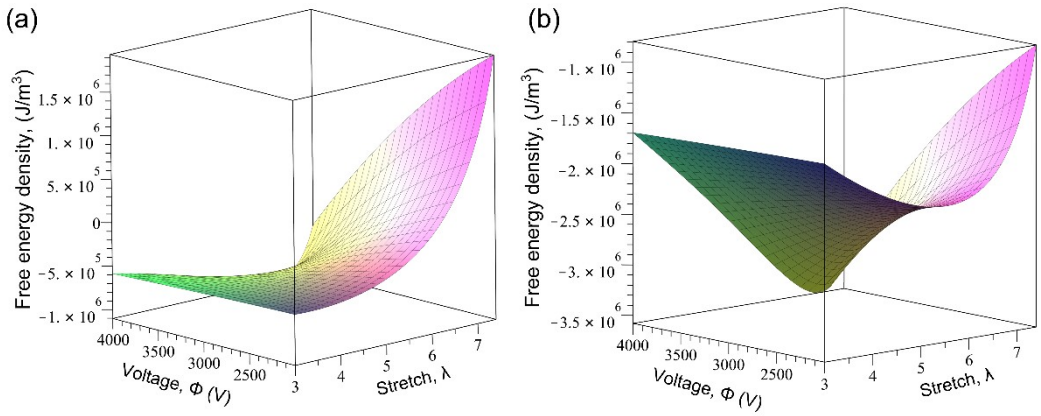

Fig. S11 The computed free energy density as a function of applied voltage and stretch for the DEAs under the pre-stretch of (a) λ_{pre}=3 and (b) λ_{pre}=5, respectively. In both scenarios, it is apparent that only one minimum exists at a certain voltage, indicative of a singular stable state during the actuation process.